AGU PUBLICATIONS

Geophysical Research Letters

RESEARCH LETTER
10.1002/2016GL071356

Key Points:
- Self-organizing maps capture downstream atmospheric responses associated with Arctic SHF patterns without use of regional metrics
- Arctic sensible heat fluxes produce low-level warming that builds and modulates eastward propagating planetary waves
- Robust near-surface temperature anomalies in the United States last approximately 2 weeks

Supporting Information:
- Supporting Information S1
- Figure S1
- Figure S2
- Figure S3
- Figure S4
- Figure S5
- Figure S6

Correspondence to:
C. M. Mills,
catrin.mills@pnnl.gov

Citation:
Mills, C. M., J. J. Cassano, and E. N. Cassano (2016), Midlatitude atmospheric responses to Arctic sensible heat flux anomalies in Community Climate Model, Version 4, *Geophys. Res. Lett.*, *43*, 12,270–12,277, doi:10.1002/2016GL071356.

Received 29 SEP 2016
Accepted 2 NOV 2016
Accepted article online 4 NOV 2016
Published online 10 DEC 2016

Midlatitude atmospheric responses to Arctic sensible heat flux anomalies in Community Climate Model, Version 4

Catrin M. Mills[1,2], John J. Cassano[3], and Elizabeth N. Cassano[2]

[1]Atmospheric Sciences and Global Change Division, Pacific Northwest National Laboratory, Richland, Washington, USA, [2]Cooperative Institute for Research in Environmental Sciences, University of Colorado, Boulder, Colorado, USA, [3]Cooperative Institute for Research in Environmental Sciences and Department of Atmospheric and Oceanic Sciences, University of Colorado Boulder, Boulder, Colorado, USA

Abstract Possible linkages between Arctic sea ice loss and midlatitude weather are strongly debated in the literature. We analyze a coupled model simulation to assess the possibility of Arctic ice variability forcing a midlatitude response, ensuring consistency between atmosphere, ocean, and ice components. We work with weekly running mean daily sensible heat fluxes with the self-organizing map technique to identify Arctic sensible heat flux anomaly patterns and the associated atmospheric response, without the need of metrics to define the Arctic forcing or measure the midlatitude response. We find that low-level warm anomalies during autumn can build planetary wave patterns that propagate downstream into the midlatitudes, creating robust surface cold anomalies in the eastern United States.

1. Introduction

Warming in the Arctic is occurring at twice the rate as the rest of the globe, while cooling trends have been observed in the eastern United States in recent years [*Cohen et al*., 2014]. Arctic ice acts to inhibit communication between the ocean and atmosphere. As the ice cover is rapidly diminishing, assessing the possibility that these changes are linked to remote midlatitude responses is a top science priority. One mechanism for connections due to Arctic warming is atmospheric circulation pattern changes, through reduction of the poleward thickness gradient and amplification of upper level waves [*Francis and Vavrus*, 2012, 2015; *Overland and Wang*, 2010; *Cvijanovic and Caldeira*, 2015].

There is increasing evidence from observational studies that sea ice loss and Arctic amplification is already having effects on midlatitude weather [e.g., *Francis and Vavrus*, 2012]. Other studies [e.g., *Screen and Simmonds*, 2013; and *Barnes*, 2013], however, have shown that results are sensitive to the metric chosen to measure upper level wave response and that downstream linkages cannot be statistically proven [*Hopsch et al*., 2012]. Natural atmospheric variability camouflages signals associated with physical mechanisms linking changes to midlatitude responses in observations [*Walsh*, 2014; *Overland et al*., 2015]. Another area of complexity is that the regional ice variability may have different impacts on downstream responses depending on where it occurs (e.g., impacts on Greenland blocking highs versus roles of the North Pacific) [also see *Kug et al*., 2015].

Since observations are sparse in the Arctic and response signals may be covered by noise associated with interannual variability, modeling studies can be useful and have also shown that diminishing ice cover and Arctic warming are associated with midlatitude atmospheric (cooling) responses [e.g., *Deser et al*., 2010], but these findings have also been tempered by other modeling studies [*Screen et al*., 2013]. Studies utilizing the same climate models can even have contrasting outcomes [*Vihma*, 2014]. Currently, a robust dynamical connection between Arctic ice loss and downstream weather has not been found.

Considering these difficulties, we propose a physically motivated study that focuses on upward sensible surface heat flux (SHF) anomalies in the Arctic since the atmosphere will respond to heat fluxes associated with a diminishing and thinning ice cover, as opposed to the ice state directly. Coupled model output will be used so that we have physically consistent fluxes between the ocean, ice, and atmosphere. We chose SHF anomalies, as opposed to latent heat flux or surface longwave forcing variables, since we are interested in the direct forcing from open ocean and thin sea ice. SHF fields also showed the most prominent and

coherent anomalies, whereas LHF fields showed little to no signal. Investigation into why LHF anomalies are not more prominent is outside the scope of this paper but will be an area of future research.

We make use of self-organizing maps (SOMs) to categorize upward SHF anomalies over the Arctic. This ensures that the dominant SHF anomaly patterns are objectively identified and avoids the need to define arbitrary regions of the Arctic or sea ice loss metrics. Composites of the atmosphere and ice state, at leads (with the SHF pattern leading the composite variables of interest) up to 12 weeks, are calculated for each SOM-identified SHF anomaly pattern.

2. Data and Methods

2.1. CCSM4

Model output from the Community Climate System Model, Version 4, which has been shown to realistically represent the current Arctic atmosphere and observed changes over recent decades [*de Boer et al*., 2011], is analyzed. CCSM4 is a fully coupled model consisting of atmosphere (Community Atmosphere Model), land (Community Land Model), ocean (Parallel Ocean Program), and sea ice (Community Ice CodE) component models [*Gent et al*., 2011]. Atmosphere and ice variables from September to February were extracted for the years 1974–2005 from an ensemble member that had numerous daily output variables (r6i1p1, from the historical simulation (1850–2005)). To facilitate analysis independent of model resolution, the data set was horizontally interpolated to a 50 km Equal-Area Scalable Earth grid [*Armstrong et al*., 1997].

2.2. Self-Organizing Maps (SOMs)

The self-organizing map (SOM) [*Kohonen*, 2001] algorithm employs a neural network method that uses unsupervised learning to determine generalized patterns in data. This technique reduces the dimensionality of large data sets by grouping similar data records together and organizing them into a two-dimensional array that becomes a mapping of the pattern space occupied by the input data. It can also be useful to think of the technique as a nonlinear take on principal component analysis because the SOM technique does not have the orthogonality constraint and can better extract patterns in a given data set [*Reusch et al*., 2005]. This methodology has been used in many disciplines and is becoming more widely used in the atmospheric sciences [e.g., *Hewitson and Crane*, 2002; *Cassano et al*., 2015; *Mills and Walsh*, 2014; *Sheridan and Lee*, 2011; *Huth et al*., 2008]. For the current work, the SOM technique was used to classify the autumn (September–November) weekly running mean anomalies of daily upward SHF from the long-term daily mean since the atmosphere will most likely respond to sustained heat fluxes (e.g., the weekly running mean daily SHF anomaly pattern for 10 September of a given year is calculated from the daily SHF anomaly fields for 7, 8, 9, 10, 11, 12, and 13 September of that year). The six SHF anomaly patterns identified by the SOM algorithm are shown in supporting information Figure S1. SOM sizes ranging from 6 maps to 20 maps were analyzed, and the six SHF anomaly patterns provided the best balance of generalization of patterns while still accurately clustering different patterns. Climatologically open water areas were masked to focus on newly exposed Arctic Ocean regions because we are interested in assessing how changes in ice coverage influence climate. Figure 1 shows the SHF pattern that exhibited the most prominent, coherent downstream atmospheric signals analyzed. Positive (upward) SHF anomalies are most prominent in the Beaufort-Chukchi Seas region, with anomalies of approximately 12 W/m^2 near the coast of Barrow, extending from the Canadian Archipelago to the Chukchi Sea.

3. Results: Weekly Lead Atmospheric Composites

Once a SOM is created, each data sample used to create the SOM can be compared with each pattern to determine which pattern it most closely matches, providing a list of dates associated with each SOM pattern. This can then be used to create composite fields for concurrent and weekly leading variables for each pattern in the SOM (supporting information Figure S1), analogous to *Cassano et al*. [2007]. This characterization allows us to assess the atmospheric state concurrent with and after the initial SHF signal and to assess the timescale of possible downstream atmospheric responses.

Composite fields for concurrent patterns, or zero lead, are shown in Figure 2. Here we will use *lead* since the Master SOM SHF pattern in Figure 1 leads the variables shown in the subsequent figures (sensible heat flux, sea ice thickness and concentration, surface and 700 hPa air temperature, 1000–500 hPa thicknesses, sea level pressure, and geopotential heights at 500 hPa and 250 hPa). These figures indicate responses in

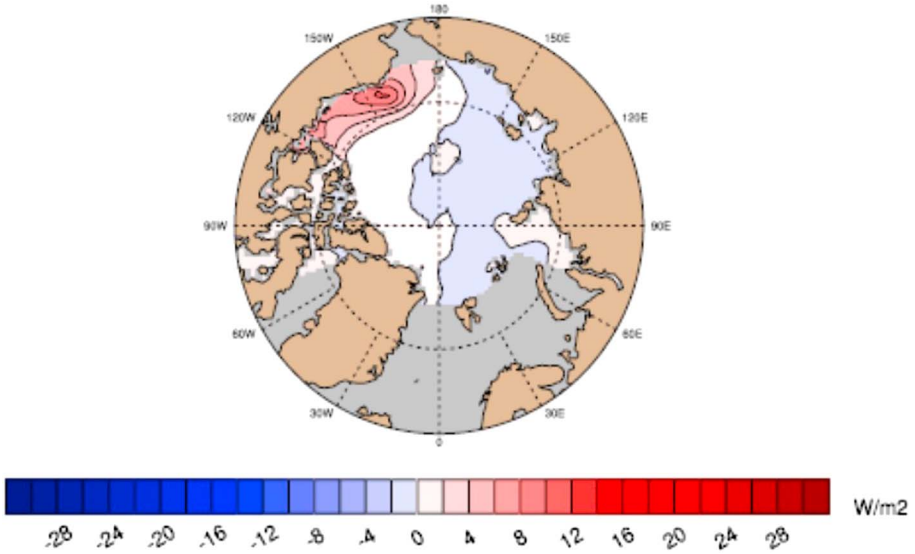

Figure 1. The bottom-right pattern from the Master SOM of upward sensible heat flux anomaly (W/m^2) patterns in the Arctic (supporting information Figure S1). This is the node of focus in the subsequent figures.

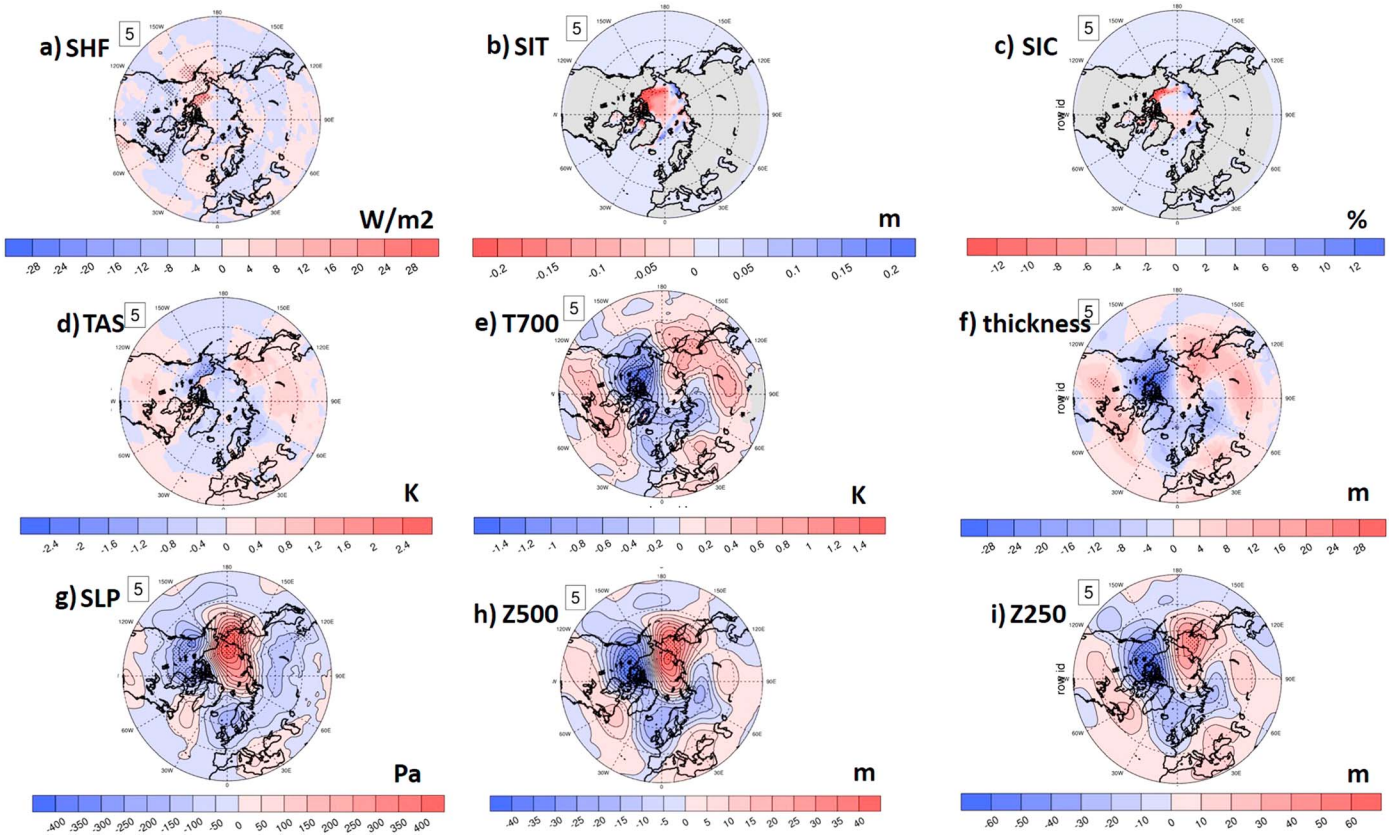

Figure 2. Composite atmospheric fields created by compositing anomaly fields for the days clustered on the SHF SOM pattern in Figure 1: (a) sensible heat flux (SHF) (W/m^2), (b) sea ice thickness (SIT) (m), (c) sea ice concentration (SIC) (%), (d) near-surface air temperature (SAT) (K), (e) 700 hPa air temperature (T700) (K), (f) 1000–500 hPa thickness (m), (g) sea level pressure (SLP) (Pa), (h) 500 hPa geopotential heights (Z500) (m), and (i) 250 hPa geopotential heights (Z250) (m), created by compositing the given anomaly fields for the days clustered on the SHF SOM pattern in Figure 1. Stippling indicates statistical significance at or greater than 95%.

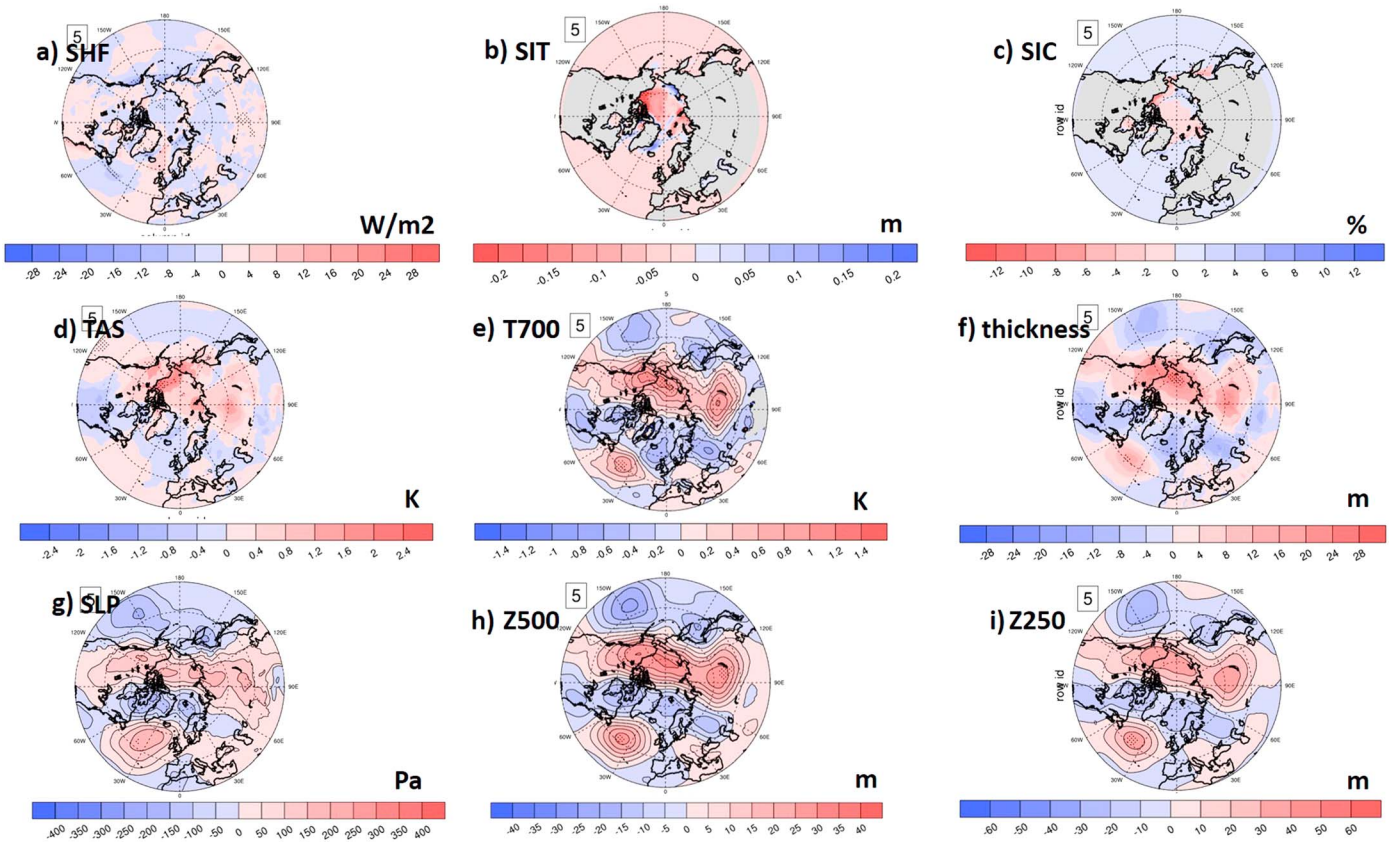

Figure 3. As in Figure 2, except that they are created by compositing the given anomaly patterns occurring 6 weeks after the days clustered on the SHF SOM pattern in Figure 1.

atmospheric state and sea ice to changes in sensible heat flux over multiple lead times. Statistical significance of the atmospheric responses was calculated for the composite fields for a given variable relative to the long-term mean field (effective sample sizes, calculated from the lag-1 autocorrelation, were used for the sample sizes for the long-term mean fields). To further ensure that the weekly leading atmospheric responses were not random occurrences or erroneously calculated as robust (i.e., that no other randomly chosen sample of composited daily SHF fields were calculated as statistically significant at 95%), we conducted random resampling experiments testing the statistical significance of randomly chosen composite daily SHF fields relative to the long-term mean field. Thousands of random samples of atmospheric fields were generated with the constraint that the sample has to be the same size as the studied sample generated by the SOM analysis (similar to a random permutation or a Monte Carlo test). Analogous statistical significance values were calculated for these random samples, with none being statistically significant. We have not attempted to explain the physical sources for the SHF anomalies. We are only interested in the downstream atmospheric response associated with local Arctic SHF patterns, regardless of their physical origin.

Robust positive sensible heat flux anomalies and negative ice thickness and ice concentration anomalies are present in a narrow region north of Alaska (Figure 2). This zero lead represents the atmospheric state associated with SOM pattern in Figure 1 (as can be seen by comparison to the SHF pattern in Figure 2). At zero lead, cold near-surface air temperature anomalies are located above the positive sensible heat flux anomaly pattern in the Beaufort-Chukchi Seas region (associated with cold-air advection driven by low SLP over Alaska and high SLP over the Bering Strait, which is also visible in the upper levels at 700, 500, and 250 hPa). The cold air over low ice concentration/thin ice results in upward heat transfer from the ocean to the atmosphere [*Honda et al.*, 2009; *Liptak and Strong*, 2014]. Two weeks after the initial SHF anomaly (2 week lead), the initial sensible heat flux anomaly pattern has produced low-level warming not yet apparent in the upper levels, while the SHF anomaly gradually weakens with time (Figure S2).

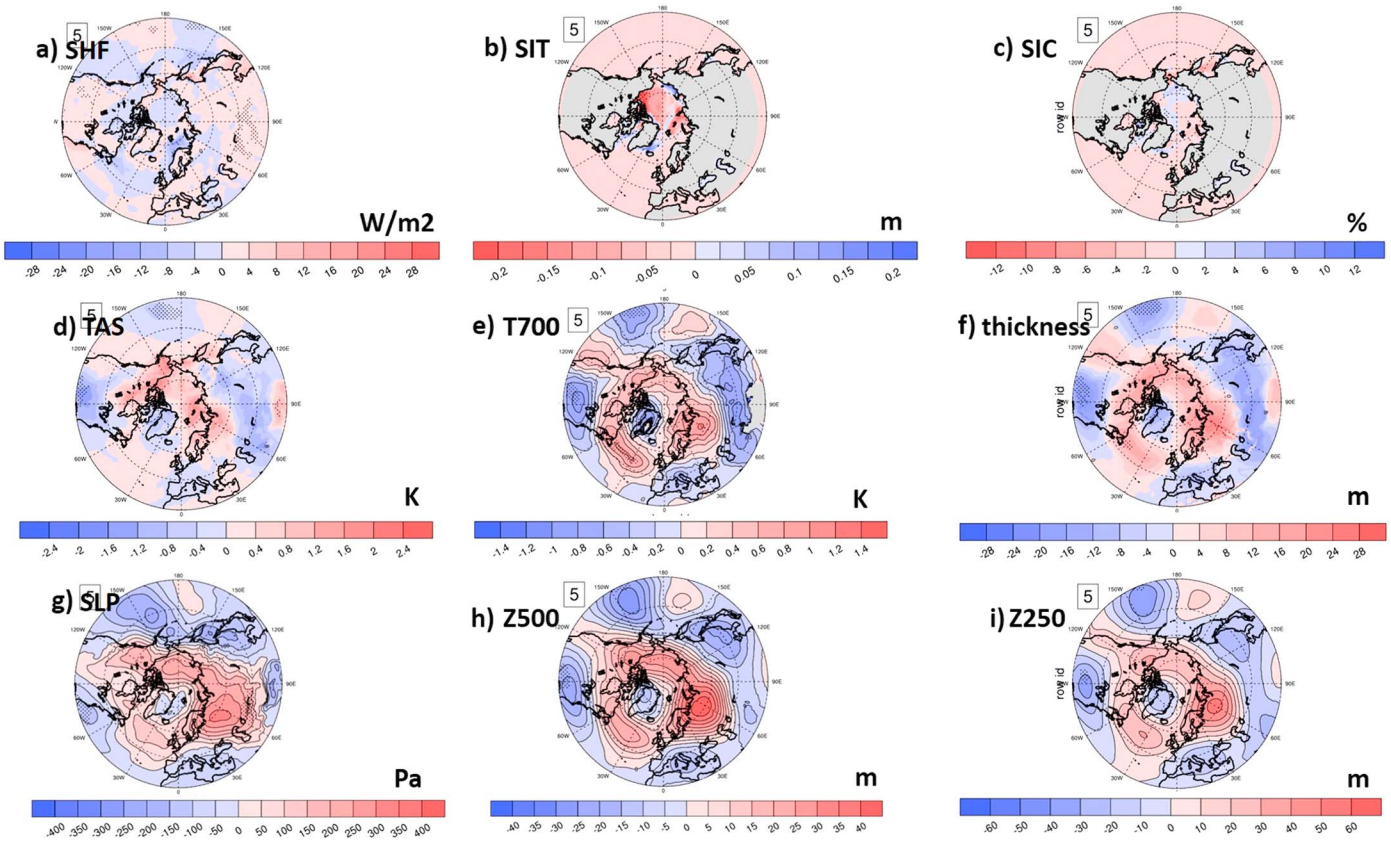

Figure 4. As in Figure 2, except that they are created by compositing the given anomaly patterns occurring 8 weeks after the days clustered on the SHF SOM pattern in Figure 1.

In the 4 week lead composite fields (Figure S3), the sensible heat flux signal has further weakened, except a narrow portion just north of Alaska. The warm surface air temperature signal northeast of Alaska has deepened with evidence of this warming at 700 hPa and in the 1000–500 hPa thickness. This deep warming has propagated eastward of the initial sensible heat flux anomaly signal and is collocated with the upper level ridging at 500 hPa and 250 hPa.

A ridge-trough-ridge wave train at 500 and 250 hPa is evident in the 6 week lead composite fields, shown in Figure 3, with the dominant ridge collocated with the warm atmospheric anomalies from the surface through 500 hPa north of Alaska over the region of the initial positive SHF anomalies. The trough in the wave train is located over eastern North America. Cold surface temperatures in eastern North America are located downstream of the SLP ridging in western North America, consistent with cold-air advection, and collocated with the upper level trough.

The negative temperature anomalies over eastern North America for the 6 week lead (Figure 3) have become statistically significant 8 weeks after the initial SHF pattern (Figure 4). There exists coherence between the persistent thin-ice concentration, vertically stacked warm anomalies near Alaska, and the upper level ridging. The cold anomalies over the eastern United States continue to build into week 9 (Figure 5) and are physically consistent with the forcing seen in earlier lead composites. As with earlier composites, these cold anomalies over the East Coast are likely strengthened via cold-air advection from the positive SLP anomaly, downstream of the 500 hPa ridge which is driven by the warm anomalies over and downstream of Alaska.

Kug et al. [2015] also find that western Arctic ice loss is associated with downstream atmospheric responses in North America (although their ice loss is slightly shifted eastward over the Siberian Sea); however, the responses they see are on shorter timescales. Interestingly, the timescales of the responses are similar to those found in *Kim et al.* [2014]; however, they propose a stratospheric mechanism, while the response is

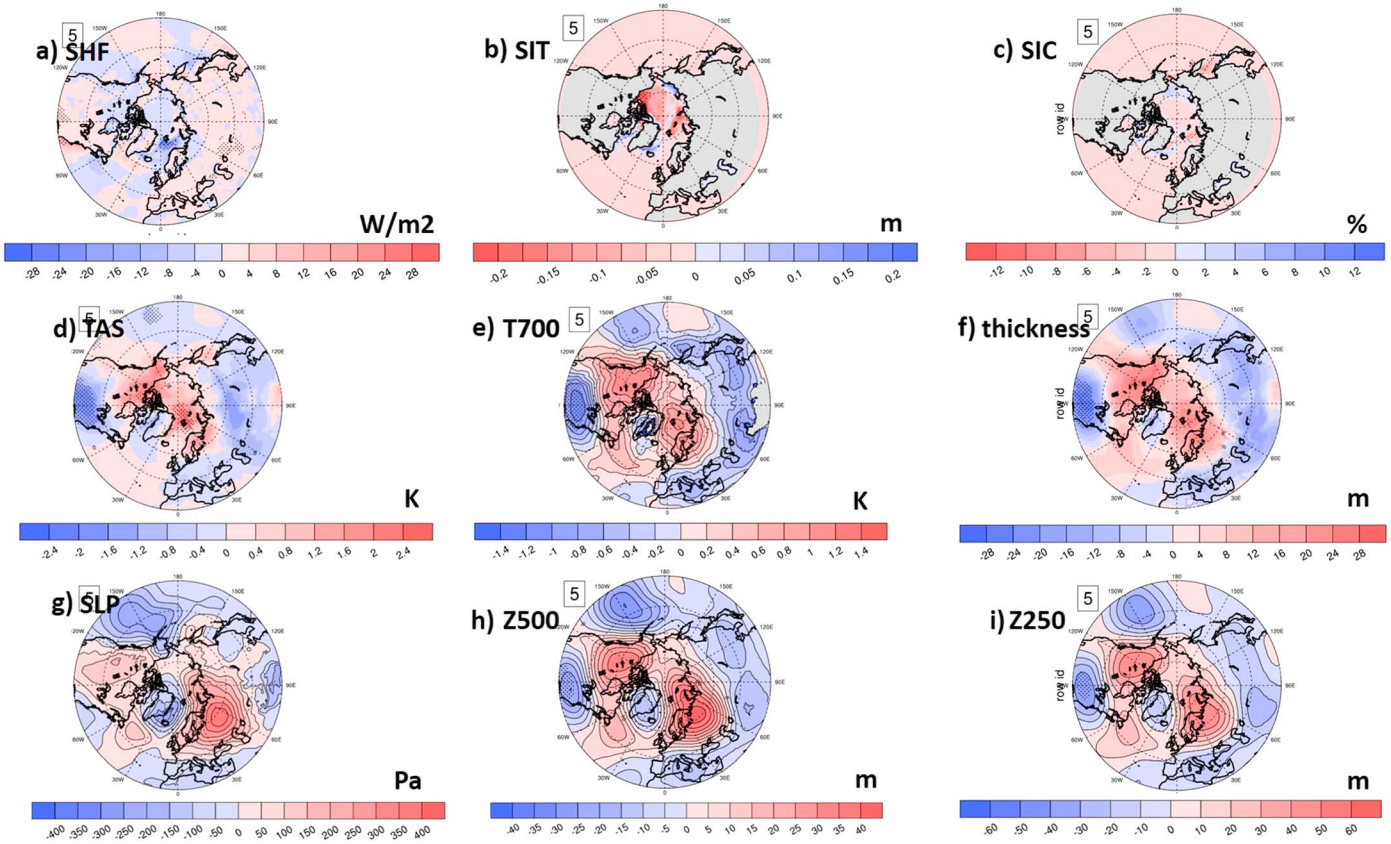

Figure 5. As in Figure 2, except that they are created by compositing the given anomaly patterns occurring 9 weeks after the days clustered on the SHF SOM pattern in Figure 1.

initiated by low-level changes. In general, SLP fields are less coherent than the upper level fields, and this may be associated with greater variability in the surface pressure fields [*Overland and Wang*, 2010]. The surface and upper level signals over the entire domain rapidly weaken by week 10, seen in Figure S4.

Other SHF anomaly patterns identified by the SOM (Figure S1) were not found to be associated with as clear a midlatitude response as seen for SOM pattern 5 described above. In pattern 2 the sea ice thickness anomalies (Figure S5) are concentrated farther eastward over the Chukchi and Eastern Siberian Seas than for pattern 5. Identifying why some ice free or thin-ice regions (and thus SHF patterns) are more important than others in exciting downstream responses is not the focus of the present study but is planned for future research. If we assume that analogous physical mechanisms occur on similar timescales to build low-level heating above the respective SHF anomalies for both patterns, it appears that the lead responses associated with pattern 2, shown in Figure S6a–S6c, are more zonal and confined to the Arctic as the lower level heating builds in weeks 6 to 8 than compared to pattern 5. (However, considering that the composite variables associated with this pattern are neither physically coherent nor statistically significant over the United States, it could simply be that the downstream responses do not evolve in a coherent manner, on average.)

4. Conclusions

Through the use of a coupled climate model and SOMs this study explores potential impacts of Arctic ice loss/variability on weather in the midlatitudes. Use of a coupled model ensures consistent fluxes between the ice, ocean, and atmosphere. Utilizing the modeled SHFs allows us to expose the local atmospheric response to heating driven by ice loss, while the weekly lead composites allow us to document how this local response expands across the Arctic and the midlatitudes on intraseasonal timescales. Although global climate models have had issues producing the observed sea ice decline [*Stroeve et al.*, 2007] and have low

resolution that may not resolve important regional features, the analysis presented here allows us to capture complex downstream connections.

The SOM technique depicts prominent SHF patterns in the Arctic and allows us to examine weekly lead atmospheric response without the use of a potentially arbitrary metric or analysis region. This is particularly useful since teleconnections may not only be excited by maximum ice loss but also by some sufficient (i.e., lower amplitude) ice loss that allows communication between the ocean and atmosphere. It is also important to note that the model output is from a free-running general circulation model (GCM) that is not forced by prescribed ice or sea surface temperatures, which generally have not been able to simulate these responses [*Cohen et al*., 2014]. Composite weekly lead fields show coherent temporal progressions between forcing, temperature anomalies, and circulation anomalies. Positive sensible heat flux anomalies in the Barents and Chukchi Seas produce local low-level warm anomalies that build an upper level ridge and excite a planetary wave train. This robust planetary wave response downstream of the heat flux pattern peak about 8 weeks after the initial SHF signal is associated with cold-air advection in eastern North America and last for approximately 2 weeks, before rapidly breaking down. The mechanism in the present study appears to be lower level sensible heat fluxes producing low-level warming that builds and modulates eastward propagating planetary waves [*Serreze et al*., 2009, 2011; *Stroeve et al*., 2012]. An in-depth analysis of what causes the differences of timescales of the responses [e.g., *Kim et al*., 2014] and what ingredients are necessary to excite downstream responses is a path of future research.

Persistent sea ice thicknesses may be important in forcing the atmospheric responses, highlighting the utility of using coupled GCM output and that regional ice conditions are important to identifying downstream connections [*Kug et al*., 2015]. Future work will apply the method used here to investigate the role of Arctic surface anomalies in forcing midlatitude weather in multiple reanalyses and an ensemble of Coupled Model Intercomparison Project models to assess if the results presented above are robust across multiple data sets. In addition, targeted modeling studies will be used to investigate the role of the regionality of sea ice conditions in forcing downstream responses.

Acknowledgments
This work was supported in part by NASA grant NNX14AH89G and the University of Colorado Cooperative Institute for Research in Environmental Sciences (CIRES) Visiting Fellows program. C. Mills also acknowledges support from the DOE, Office of Science, Biological and Environmental Research as part of the Regional and Global Climate Modeling program. The Pacific Northwest National Laboratory (PNNL) is operated for DOE by Battelle Memorial Institute under contract DE-AC05-76RLO1830. The NCAR CCSM4 model output used for the analysis is available at http://www.cesm.ucar.edu/experiments/cesm1.0/. We thank the two anonymous reviewers for their time and useful comments that helped improve this manuscript.

References

Armstrong, R., M. J. Brodzik, and A. Varani (1997), The NSIDC EASE-Grid: Addressing the need for a common, flexible, mapping and gridding scheme, *Earth Syst. Monitor*, *7*(4), 3.

Barnes, E. A. (2013), Revisiting the evidence linking Arctic amplification to extreme weather in midlatitudes, *Geophys. Res. Lett.*, *40*, 4734–4739, doi:10.1002/grl.50880.

Cassano, E., J. Glisan, J. Cassano, W. J. Gutowski, and M. Seefeldt (2015), Self-organizing map analysis of widespread temperature extremes in Alaska and Canada, *Clim. Res.*, *62*(3), 199–218, doi:10.3354/cr01274.

Cassano, J. J., P. Uotila, A. H. Lynch, and E. N. Cassano (2007), Predicted changes in synoptic forcing of net precipitation in large Arctic river basins during the 21st century, *J. Geophys. Res.*, *112*, G04S49, doi:10.1029/2006JG000332.

Cohen, J., et al. (2014), Recent Arctic amplification and extreme mid-latitude weather, *Nature Geosci.*, *7*, 627–637.

Cvijanovic, I., and K. Caldeira (2015), Atmospheric impacts of sea ice decline in CO_2 induced global warming, *Clim. Dyn.*, *44*, 1173–1186.

de Boer, G., W. Chapman, J. E. Kay, B. Medeiros, M. D. Shupe, S. Vavrus, and J. Walsh (2011), A characterization of the present-day arctic atmosphere in CCSM4, *J. Clim.*, *25*(8), 2676–2695, doi:10.1175/jcli-d-11-00228.1.

Deser, C., R. Tomas, M. Alexander, and D. Lawrence (2010), The seasonal atmospheric response to projected Arctic sea ice loss in the late twenty-first century, *J. Clim.*, *23*(2), 333–351, doi:10.1175/2009jcli3053.1.

Francis, J. A., and S. J. Vavrus (2012), Evidence linking Arctic amplification to extreme weather in mid-latitudes, *Geophys. Res. Lett.*, *39*, L06891, doi:10.1029/2012GL051000.

Francis, J. A., and S. J. Vavrus (2015), Evidence for a wavier jet stream in response to rapid Arctic warming, *Environ. Res. Lett.*, *10*(1), 014005, doi:10.1088/1748-9326/10/1/014005.

Gent, P. R., et al. (2011), The Community Climate System Model Version 4, *J. Clim.*, *24*(19), 4973–4991, doi:10.1175/2011jcli4083.1.

Hewitson, B. C., and R. G. Crane (2002), Self-organizing maps: Applications to synoptic climatology, *Clim. Res.*, *22*(1), 13–26, doi:10.3354/cr022013.

Honda, M., J. Inoue, and S. Yamane (2009), Influence of low Arctic sea-ice minima on anomalously cold Eurasian winters, *Geophys. Res. Lett.*, *36*, L08707, doi:10.1029/2008GL037079.

Hopsch, S., J. Cohen, and K. Dethloff (2012), Analysis of a link between fall Arctic sea ice concentration and atmospheric patterns in the following winter, *Tellus A*, *2012*, 64, doi:10.3402/tellusa.v64i0.18624.

Huth, R., C. Beck, A. Philipp, M. Demuzere, Z. Ustrnul, M. Cahynová, J. Kyselý, and O. E. Tveito (2008), Classifications of atmospheric circulation patterns, *Ann. N. Y. Acad. Sci.*, *1146*(1), 105–152, doi:10.1196/annals.1446.019.

Kim, B.-M., S.-W. Son, S.-K. Min, J.-H. Jeong, S.-J. Kim, X. Zhang, T. Shim, and J.-H. Yoon (2014), Weakening of the stratospheric polar vortex by Arctic sea-ice loss, *Nat. Commun.*, *5*, 4646, doi:10.1038/ncomms5646.

Kohonen, T. (2001), Self-organizing maps, in *Self-Organizing Maps*, *Springer Series in Information Sciences*, 3rd ed., 501 pp., Springer, Berlin.

Kug, J.-S., J.-H. Jeong, Y.-S. Jang, B.-M. Kim, C. K. Folland, S.-K. Min, and S.-W. Son (2015), Two distinct influences of Arctic warming on cold winters over North America and East Asia, *Nat. Geosci.*, *8*(10), 759–762, doi:10.1038/ngeo2517.

Liptak, J., and C. Strong (2014), The winter atmospheric response to sea ice anomalies in the Barents Sea, *J. Clim.*, *27*(2), 914–924, doi:10.1175/JCLI-D-13-00186.1.

Mills, C. M., and J. E. Walsh (2014), Synoptic activity associated with sea ice variability in the Arctic, *J. Geophys. Res. Atmos.*, *119*, 12,117–12,131, doi:10.1002/2014JD021604.
Overland, J. E., and M. Y. Wang (2010), Large-scale atmospheric circulation changes are associated with the recent loss of Arctic sea ice, *Tellus A*, *62*(1), 1–9, doi:10.1111/J.1600-0870.2009.00421.X.
Overland, J., et al. (2015), The melting Arctic and midlatitude weather patterns: are they connected?, *J. Clim.*, *28*, 7917–7932.
Reusch, D. B., R. B. Alley, and B. C. Hewitson (2005), Relative performance of self-organizing maps and principal component analysis in pattern extraction from synthetic climatological data, *Polar Geogr.*, *29*(3), 188–212, doi:10.1080/789610199.
Screen, J. A., and I. Simmonds (2013), Caution needed when linking weather extremes to amplified planetary waves, *Proc. Natl. Acad. Sci. U.S.A.*, *110*(26), E2327, doi:10.1073/pnas.1304867110.
Screen, J. A., I. Simmonds, C. Deser, and R. Tomas (2013), The atmospheric response to three decades of observed arctic sea ice loss, *J. Clim.*, *26*(4), 1230–1248, doi:10.1175/jcli-d-12-00063.1.
Serreze, M. C., A. P. Barrett, and J. J. Cassano (2011), Circulation and surface controls on the lower tropospheric air temperature field of the Arctic, *J. Geophys. Res.*, *116*, D07104, doi:10.1029/2010JD015127.
Serreze, M., A. Barrett, J. Stroeve, D. Kindig, and M. Holland (2009), The emergence of surface-based Arctic amplification, *Cryosphere*, *3*(1), 11–19.
Sheridan, S. C., and C. C. Lee (2011), The self-organizing map in synoptic climatological research, *Prog. Phys. Geogr.*, *35*(1), 109–119, doi:10.1177/0309133310397582.
Stroeve, J., M. M. Holland, W. Meier, T. Scambos, and M. Serreze (2007), Arctic sea ice decline: Faster than forecast, *Geophys. Res. Lett.*, *34*, L09501, doi:10.1029/2007GL029703.
Stroeve, J. C., et al. (2012), The Arctic's rapidly shrinking sea ice cover: A research synthesis, Clim. *Change*, *110*, 1005–1027.
Vihma, T. (2014), Effects of Arctic sea ice decline on weather and climate: a review, *Surv. Geophys.*, *35*(5), 1175–1214, doi:10.1007/s10712-014-9284-0.
Walsh, J. E. (2014), Intensified warming of the Arctic: Causes and impacts on middle latitudes, *Global Planet. Change*, *117*, 52–63, doi:10.1016/j.gloplacha.2014.03.003.